Determination of the Potential of Mean Force of Aromatic Amino Acid Complexes in Various Solvents Using Molecular Dynamics Simulations: The Case of the Tryptophan−Histidine Pair

Francesco Luigi Gervasio, Riccardo Chelli, Massimo Marchi,† Piero Procacci,* and Vincenzo Schettino

Università di Firenze, Dipartimento di Chimica, Via Gino Capponi 9, I-50121 Firenze, Italy, and European Laboratory for Nonlinear Spectroscopy (LENS), Largo E. Fermi 2 I-50125 Firenze, Italy

An analysis of structural properties of the tryptophan−histidine (TRP−HIS) pair in vacuo and in various solvents (water, dimethyl sulfoxide, methanol, and carbon tetrachloride) has been done using classical molecular dynamics simulations with atomistic potential models for both solute and solvent molecules. The potential of mean force (PMF) was determined as a function of the TRP centroid−HIS centroid distance and of the angle between the ring planes. We show that T-shaped structures are favored in nonpolar solvents, whereas they are completely destabilized in solvents forming strong hydrogen bonds. Amphiphilic solvents such as methanol and dimethyl sulfoxide destabilize both the T-shaped and stacked arrangements. The results are consistent with previous analysis on protein crystallographic databases, where the stacked structures are found mainly on the protein surface exposed to the solvent, while T-shaped arrangements are preferentially found in the hydrophobic protein core. Finally, comparison of explicit solvent molecular simulation data and continuum solvent model results emphasizes the importance of microsolvation phenomena in shaping the potential of mean force for tryptophan−histidine interactions.

I. Introduction

Interactions between aromatic residues are important for the structural properties of biological systems. Base stacking, for example, plays a fundamental role in stabilizing the helical structure of nucleic acids. In proteins, aromatic residues such as tyrosine, tryptophan, phenylalanine, and, to a smaller extent, histidine tend to be buried in the hydrophobic core. Aromatic−aromatic interactions involving some of these residues are frequently found to link distinct secondary structure elements.[1] This suggests that they may largely contribute in stabilizing protein tertiary structure and, hence, may be important in driving the folding process. In a survey[1] of 34 protein structures where about 300 contact structures of aromatic residues pairs were analyzed, the angles between the aromatic rings and the distances between the centroids were found to be consistent with T-shaped structures, with the planes of the rings perpendicular to each other. It was later on suggested that aromatic rings in proteins could act as hydrogen bond (H-bond) acceptors.[2] When these unconventional H-bonds are established between aromatic pairs, the T-shaped arrangement[2,3] is stabilized through the formation of a directional (perpendicular to the ring) interaction between proton group donors (such as the amino group in histidine or tryptophan) and the partner aromatic ring. In another study[4] on 55 nonhomologous high-resolution protein chain structures where amino-aromatic interactions were surveyed, Mitchell et al. questioned the importance of H-bonds involving the aromatic ring, showing that, e.g., histidine, a residue generally exposed to the solvent, interacts with tyrosine and phenylalanine, forming preferentially stacked arrangements stabilized by the formation of conventional solvent-residue H-bonds.

All these statistical studies on coordinates data sets[1,4,5] are ultimately aimed at probing differences in the free energy of aromatic−aromatic structures in a protein environment. Overall, they all seem to suggest that there exists a competition between stacked and T-shaped or crossed structures and that this competition is strongly affected by the polarity of the environment and the ability of the surrounding solvent to form H-bond.

From a theoretical standpoint, aromatic−aromatic interactions have been intensively studied using semiempirical and ab initio techniques.[6−8] Most of these investigations were focused on the energetics and structure of stationary points in vacuo. Stationary point calculations using accurate ab initio methods, such as Møller Plesset second-order perturbation theory[9] (MP2) combined with polarizable continuum model[10,11] for including the effect of polarizable dielectrics, could be in principle a valuable tool in determining the preferential conformations of these molecules at finite temperature and in polar solvents. However, besides the inherent approximations such as the cavity shape and the truncation level for electrostatic sums,[12] the continuum polarizable model suffers of a major shortcoming: the microsolvation effects due to the atomic details, e.g., the presence of functional groups with hydrophobic and/or hydrophilic character, are totally neglected. Evidently, this approximation is unrealistic in many instances (when, e.g., the H-bonding is an essential feature of the solvation effect), and it does indeed have a strong impact on both the energetic and entropic contributions to the free energy. While relative stabilization energies are certainly strongly affected by persistent solute−solvent H-bonds or other specific solute−solvent interactions, the distribution of the solute vibrational frequencies, which is important for the thermal

* To whom correspondence should be addressed. E-mail: procacci@chim.unifi.it.

† Permanent addrress: Section de Biophysique des Protéines et des Membranes, DBCM, DSV, CEA, Centre d′Études, Saclay, 91191 Gif-sur-Yvette Cedex, France.

10.1021/jp010434w CCC: $20.00
Published on Web 07/25/2001

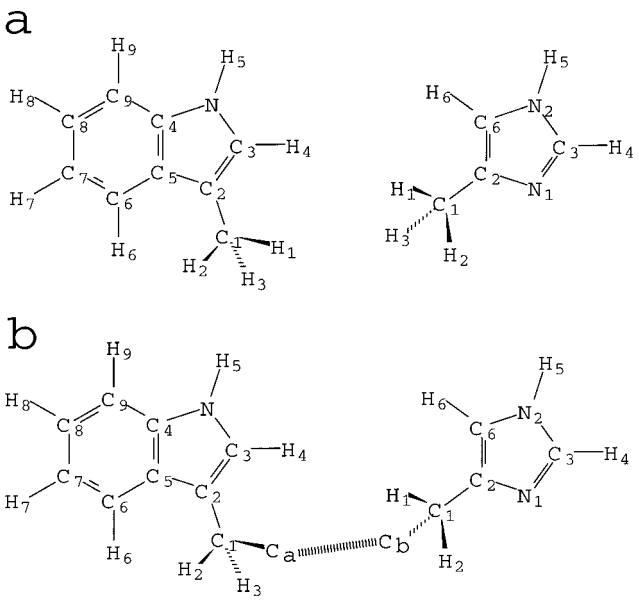

Figure 1. (a) Methyl indole (TRP, left side) and methyl imidazole (HIS, right side) structures. This pair is referred in the text as the "TRP−HIS unbound complex". (b) Ethyl indole (TRP, left side) and ethyl imidazole (HIS, right side) structures. This pair is referred in the text as the "TRP−HIS bound complex". As shown, the constraint is between the C_a atom of TRP and the C_b atom of HIS.

contribution to the free energy, may also be affected by specific solute−solvent interactions.

Classical molecular dynamics simulations using realistic potential models can in principle be of great help in elucidating the free energy landscape in specific and controlled thermodynamic conditions as a function of the solvent polarity. To our knowledge, systematic calculations of this kind on aromatic amino acids are not available in the literature. By using Monte Carlo simulation, Jorgensen and Severance[13] have investigated the potential of mean force (PMF) for the benzene dimer in water and chloroform. They found that the dimer T-shaped structures are favored in both cases at room conditions. However, they obtained clear indications that stacked structures become increasingly favorable with increasing arene size. On the other hand, for aromatic residues, the free energy landscape may be entirely different due to the possibility of formation of conventional or unconventional solute−solute or solute−solvent H-bonds. This is the case of indole and imidazole derivatives, which are the object of the present paper.

Classical molecular dynamics has been used here to investigate the structural properties and interactions of the methyl indole and methyl imidazole pair (TRP−HIS unbound complex) and their ethylate bound counterparts (TRP−HIS bound complex) in various solvents (see Figure 1). The indole and imidazole groups are the characteristic side chains of the tryptophan and histidine protein residues, respectively. The PMF of the TRP−HIS unbound complex as a function of the distance R between the two ring centroids and of the dihedral angle θ between the ring planes has been determined in water, dimethyl sulfoxide (DMSO), methanol (MeOH), and carbon tetrachloride (CCl_4). The structures corresponding to the free energy minima have been characterized and discussed in terms of H-bonding, electrostatic, and dispersion interactions. In proteins, the residues are attached to a rigid backbone such that the distance between the atoms directly connected to the backbone fluctuates with a relatively small amplitude around a mean value. To simulate stereospecific effects due to this constraints, we have also determined the free energy landscape for the ethyl indole and ethyl imidazole pair by constraining the distance between the two α-carbons (see model in Figure 1b).

Molecular dynamics calculations show that solvent and constraint effects on the (R,θ) free energy surface are indeed crucial. For freely interacting methylate derivatives, polar solvents tend to stabilize the stacked arrangements, while for non polar solvents or in vacuo, the T-shaped structures are favored. For the bound complex, simulations in the same solvents at various constrained distances may show totally different free energy patterns.

The present paper is organized as follows: in section II, we discuss the potential model adopted for the solute and for the solvent as well as the methodology used in the simulations. In section III, we discuss the results obtained for the PMF of the TRP−HIS unbound complex in vacuo, CCl_4, DMSO, MeOH, and water. In section III, we analyze the effect of the constraints on the free energy of the TRP−HIS bound complex in the same solvents. Finally, in section IV, conclusive remarks are presented.

II. Methods

A. Inter- and Intramolecular Potential. Classical molecular dynamics simulations are done for the methyl indole and methyl imidazole unbound complex (Figure 1a) and for the ethylate complexes with the α-carbons constrained to oscillate around selected distances (Figure 1b). More details on how and why these distances were selected are given in section III. The potential model adopted for both the solute (TRP−HIS complex) and the solvents is based on the AMBER force field.[14] In a preceding paper,[15] we studied the interaction between ethyl indole and ethyl imidazole in vacuo. We showed that the AMBER suite reproduces well the ab initio energy of some low-energy stacked and T-shaped structures. In the AMBER approach, electronic effects, such as polarization or charge transfer phenomena, are totally neglected. The good agreement between empirical and ab initio data for the ethyl indole−ethyl imidazole pair[15] indicates that, at least for this complex, electronic effects such as strong charge transfer or strong polarization response are not crucial for the shape of the potential energy surface. Indeed, we showed[15] that polarization effects are negligible for stacked arrangements, while they appear to play a minor role for the T-shaped structures, due to a moderate charge transfer across the H-bond between the nitrogen of ethyl imidazole and the polar hydrogen of ethyl indole. As for solute−solvent interactions, polarization effects were recently accounted for in the calculation of the solvation free energy of amides[16] using molecular dynamics in combination with the fluctuating charge model.[17−19] The conventional electrostatic energy was found[16] to be by far the largest contribution to the total solvation free energy, while the polarization contribution was small and practically independent of the solute conformation, thereby equally affecting solute conformations with no or little effect onto their free energy differences.

For the solute and two of the solvent molecules (MeOH and DMSO), the interaction potential is summarized in Table 1, where we report the AMBER atomic types and the atomic charges. On the basis of the force field database,[14] all constants referring to intra- or intermolecular potentials can be deduced from the knowledge of the molecular topology and of the atomic force field types. The atomic charges for methyl indole and methyl imidazole (Figure 1a) are computed according to the prescriptions given in ref 14, i.e., using a restrained electrostatic potential fitting[20] with the gridded electrostatic potential evalu-

TABLE 1: Potential Model for TRP−HIS Unbound and Bound Complexes and for MeOH and DMSO Solvents[a]

TRP-HIS unbound complex			TRP−HIS bound complex		
atom (TRP)	type	*q*/e	atom (TRP)	type	*q*/e
C_1	ct	−0.279601	C_a	ct	−0.035528
H_1	hc	0.086854	C_1	ct	0.118634
H_2	hc	0.086854	H_2	hc	0.013542
H_3	hc	0.086854	H_3	hc	0.003977
C_2	c*	−0.003479	C_2	c*	−0.245828
C_3	cw	−0.149198	C_3	cw	−0.109004
H_4	h4	0.170423	H_4	h4	0.168916
N	na	−0.448424	N	na	−0.415631
H_5	h	0.374061	H_5	h	0.363488
C_4	cn	0.185224	C_4	cn	0.186576
C_9	ca.	−0.221637	C_9	ca.	−0.285681
H_9	ha	0.128089	H_9	ha	0.158022
C_8	ca.	−0.130413	C_8	ca.	−0.111906
H_8	ha	0.118631	H_8	ha	0.119982
C_7	ca.	−0.150215	C_7	ca.	−0.149149
H_7	ha	0.116446	H_7	ha	0.125199
C_6	ca.	−0.212889	C_6	ca.	−0.286737
H_6	ha	0.140612	H_6	ha	0.174946
C_5	cb	0.101808	C_5	cb	0.206182
atom (HIS)	type	*q*/e	atom (HIS)	type	*q*/e
C_1	ct	−0.678340	C_b	ct	0.042330
H_1	hc	0.179362	C_1	ct	−0.156343
H_2	hc	0.179362	H_1	hc	0.042949
H_3	hc	0.179362	H_2	hc	0.042949
C_2	cc	0.537719	C_2	cc	0.355155
N_1	na	−0.581347	N_1	na	−0.503272
C_3	cr	0.153595	C_3	cr	0.145401
H_4	h5	0.117593	H_4	h5	0.099172
N_2	na	−0.284289	N_2	na	−0.249721
H_5	h	0.328415	H_5	h	0.326098
C_6	cw	−0.318048	C_6	cw	−0.339718
H_6	h4	0.186616	H_6	h4	0.195000
MeOH			DMSO		
atom	type	*q*/e	atom	type	*q*/e
C	ct	0.1955	C	ct	−0.37925
methyl H	h1	0.0164	methyl H	c1	0.134 30
O	oh	−0.6680	S	s	0.455 80
hydroxy-H	ho	0.4233	O	o	−0.50310

[a] Atom labels of the TRP−HIS complexes refer to those reported in Figure 1. The intra- and intermolecular potentials are obtained from the atom type (see type column) of the AMBER force field.[14] The atomic charges (in fraction of electron) are computed as described in the text. The interaction potentials for water and CCl_4 are taken from refs 24 and 21, respectively.

ated at the MP2/6-31G* level. The charges of the constrained complex (Figure 1b) were calculated using the same protocol applied to ethyl indole and ethyl imidazole,[15] with the charge on the terminal carbons (C_a and C_b in Figure 1b) being given by the sum of the atomic charges of the CH_3 group. This choice is the simplest way to maintain the electroneutrality on each monomer while not affecting all other charges. The potential model for CCl_4 is taken from ref 21. This potential yields a dielectric constant near to 1. For MeOH, the potential model, used also in a previous molecular dynamics simulation,[19] yields a dielectric constant of 28 at room conditions, to be compared to the experimental value[22] of 33 at 298 K. For DMSO, a bulk phase simulation of 1 ns at 300 K and room pressure gave a dielectric constant of 45, practically coincident with the experimental value[23] of 46 at 298 K. For water, we adopt the molecular geometry, the charges and the Lennard−Jones parameters of the SPC model,[24] while allowing for the extra flexibility of the bond angle. The dielectric constants for the SPC model[18] is 68, in fair agreement with the experimental value[25] of 78 at room temperature.

TABLE 2: Summary of the Performed Simulations (see text for details)[a]

solvent	C_a-C_b	*L*
CCl_4	3.8	19.86 (0.18)
$N = 45$	5.0	19.86 (0.18)
$t = 5$ ns	6.5	19.87 (0.18)
	no bond	19.82 (0.18)
DMSO	3.8	19.45 (0.12)
$N = 58$	5.0	19.46 (0.12)
$t = 9$ ns	6.5	19.45 (0.12)
	no bond	19.42 (0.12)
MeOH	3.8	19.96 (0.16)
$N = 113$	5.0	19.97 (0.16)
$t = 8$ ns	6.5	19.97 (0.17)
	no bond	19.94 (0.16)
water	3.8	19.92 (0.13)
$N = 234$	5.0	19.92 (0.13)
$t = 7$ ns	6.5	19.92 (0.13)
	no bond	19.89 (0.13)

[a] In the first column the solvent type, the number of solvent molecules (*N*) and the run length (*t*) are reported. C_a-C_b (in Å) is the constrained distance of the TRP−HIS bound complex. The average box side-length *L* (in Å) and its standard deviation (in bracket) are reported. "No bond" rows refer to the TRP−HIS unbound complex simulations. In vacuo simulations at all constrained distance and for the unbounded complex are done in the NVT ensemble for 5 ns in a box of 19.9 Å side-length.

B. Simulation Details. All simulations, except those in vacuo, are done in the NPT ensemble (constant number of particles, pressure and temperature) using a Parrinello−Rahman isotropic barostat[26,27] and a Nosé thermostat[28] with pressure set to 1 atm and temperature to 300 K. Simulations in vacuo are done in a cubic box of 19.9 Å side-length in the NVT ensemble (constant number of particles, volume and temperature) at 300 K. For each solution, including the in vacuo case, we run four simulations, one for the unbound complex (Figure 1a) and three for the bound complex at three different C_a-C_b distances (see Figure 1b). When the solvent is present, the starting configuration of the system is generated by inserting the solute into a cubic box filled with solvent molecules. By trials and errors, the number of solvent molecules is adjusted so as to yield, at normal (solvent) density, a simulation box of about 20 Å side-length for all simulations. The systems are then let to relax at the equilibrium density at constant temperature and pressure for about 100 ps. The production stages, during which coordinates of the solute and solvent are saved and PMF's for the complexes computed, lasts from a minimum of 5 ns to a maximum of about 9 ns. In Table 2, we summarize the performed simulations and some data relative to them.

Electrostatic interactions are calculated using the smooth particle mesh Ewald method.[29] For integrating the equations of motion, we use the five time steps r-RESPA[30,31] algorithm for protein systems.[27] Only the X−H bonds (with X being any non hydrogen atom) are held fixed during the simulations, while all other intramolecular degrees of freedom, including stretchings involving non hydrogen atoms, are explicitly integrated. All calculations are done using the program ORAC.[32]

The treatment of long-range electrostatic interactions is an important issue when dealing with calculation of solvated solute. For small solute size, that is, when the amount of solvent atoms in the simulation box largely exceeds those of the solute, the most accurate electrostatic potential due to the solvent is computed using the Ewald method, where the contribution from the periodic replicas of the solute molecules, which depends on the ratio between the volume of the solute and that of the box, is subtracted out.[33−36] This finite-size correction is

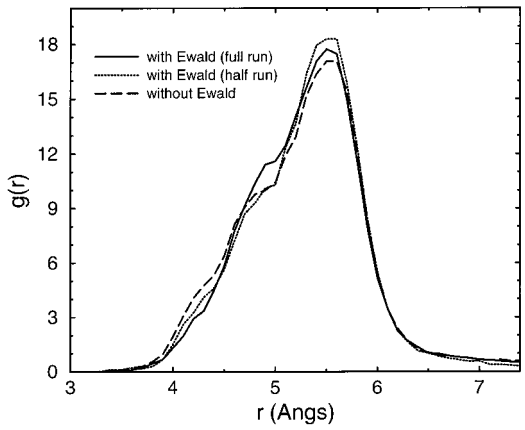

Figure 2. TRP ring centroid−HIS ring centroid radial distribution functions computed with the Ewald method (full and half runs) and with the cutoff method (see text for details).

important essentially for charged systems under periodic boundary conditions.[33,35,37] As we are dealing with neutral and relatively small solutes, we did not implement the correction due to the periodicity of the solute. However, to be on the safe side, we have compared the results obtained with the Ewald method and with the simple cutoff method for the less screened system, i.e., the TRP−HIS unbound complex in CCl_4. For this system, in the uncorrected Ewald method, the contribution of the solute replica to the total electrostatic potential is by far the largest. On the other hand, as far as the electrostatic potential is concerned, the bare cutoff method is in this case essentially exact because electrostatic interactions are indeed short-ranged, as the first nonzero multipolar moment of CCl_4 is the octupole. The TRP−HIS complex in CCl_4 is hence the ideal system for testing the effects of the solute periodicity on structural properties such as distribution functions and on the corresponding energetics given by the PMF. In Figure 2, we show the TRP ring centroid−HIS ring centroid pair distribution functions calculated from a 5 ns simulation of the TRP−HIS unbound complex in CCl_4 in a box of an average side-length of L = 19.9 Å with particle mesh Ewald and with no Ewald and a cutoff at $L/2$. The differences between the two $g(r)$'s are on the order of the statistical error, as it can be appreciated in Figure 2, where we also show the $g(r)$ computed with the Ewald method only on the first half of the simulation. Correspondingly, the PMF's obtained with the two methods (data not shown) show insignificant differences.

C. Calculation of the Potential of Mean Force. We are interested in assessing the free energy differences between the T-shaped and the stacked structures for the TRP−HIS complex in solvents of different polarity. In this respect, the mutual orientation of the TRP and HIS molecules can be described by the distance R between the centroids of the TRP and HIS rings and the angle θ between unit vectors normal to the ring planes. We limit ourselves to ascertain the relative stability of generic T-shaped and stacked structures and we do not distinguish between structures at $\pi/2 - \theta$ and $\pi/2 + \theta$. Therefore, we define a distribution function in the range $0 < \theta < \pi/2$

$$P(R,\theta) = \frac{\int e^{U(R'\theta'\mathbf{q_S},\mathbf{r_s}/k_BT}\delta(R'-R)[\delta(\theta'-\theta)+\delta(\theta'-\pi+\theta)]R'^2\sin\theta'\,dR'\,d\theta'\,d\mathbf{q_S}\,d\mathbf{r_s}}{\int e^{U(R'\theta'\mathbf{q_S},\mathbf{r_s}/k_BT}R'^2\sin\theta'\,dR'\,d\theta'\,dR'\,d\mathbf{q_S}\,d\mathbf{r_s}} = \frac{R^2\sin\theta\int e^{U(R,\theta,\mathbf{q_S},\mathbf{r_s}/k_BT}\,d\mathbf{q_S}\,d\mathbf{r_s}}{\int e^{U(R'\theta'\mathbf{q_S},\mathbf{r_s}/K_BT}R'^2\sin\theta'\,dR'\,d\theta'\,dR'\,d\mathbf{q_S}\,d\mathbf{r_s}} \quad (1)$$

where U is the configurational energy, k_B is the Boltzmann constant, T is the temperature, $\mathbf{q_S}$'s are the remaining $3N_S - 2$ independent coordinates relative to the solute, with N_S being the total number of atoms of the solute, and $\mathbf{r_s}$'s are the $3N_s$ coordinates of the solvent atoms. The distribution function $G(R,\theta) = P(R,\theta)/(R^2 \sin \theta)$ gives the probability of finding the centroids of TRP and HIS at a distance R and the angle between the normals to the rings equal to θ, irrespective of the values of all other independent solute coordinates and of the coordinates of the solvent. The associated PMF[38] is hence given by

$$W(R,\theta) = -k_BT\ln[G(R,\theta)] \quad (2)$$

The function $W(R,\theta)$ corresponds to the reversible work to bring TRP and HIS from infinite distance to the configuration (R,θ) in the solvent and in the given thermodynamic conditions. The minimum of the PMF, conventionally taken to be the zero of the PMF, corresponds to the most populated complex structure, i.e., to the state with the minimum free energy. For each simulation, we have computed numerically the numerator of eq 1 and then computed the function

$$W(R,\theta) = -k_BT\ln[G(R,\theta)/G_{max}] \quad (3)$$

where G_{max} is the maximum value of the function $G(R,\theta)$. Hereafter, the acronym PMF refers to the function $W(R,\theta)$ of eq 3.

The PMF is computed using standard NPT (NVT in vacuo) molecular dynamics with conventional Boltzmann sampling. Convergence of the function $W(R,\theta)$ is checked by subdividing the simulation into chunks of equal length and recalculating the PMF's for each of them. The average value (in the R,θ space) of the standard deviation of the N chunks calculated PMF from the whole run calculated PMF is defined as follows:

$$\sigma_N = <\{N^{-1}\sum_{i=1}^{N}[W_i(R,\theta) - W_{tot}(R,\theta)]^2\}^{1/2}> \quad (4)$$

where $W_i(R,\theta)$ is the PMF at the point R,θ calculated in the ith chunk, $W_{tot}(R,\theta)$ is the PMF at the same point computed over the whole run, and the angular brackets indicate the average on the R,θ space. σ_N gives an estimate of the error of the method (see section IIIA).

III. Results and Discussion

A. Potential of Mean Force and Structural Properties of the Unbound Complex. The configurational space spanned by the unbound complex is obviously much larger than that spanned by the bound one. In the former case, the box size is used as a parameter for accelerating the sampling of the configurational space in a standard Boltzmann sampling simulation such as ours. To avoid finite-size effects, the box side-length L must be chosen large enough in such a way that the maximum distance $L/2$ corresponds to flat regions of PMF. At the same time, to reduce the configurational space to be sampled, we must also choose the side-length to be as small as possible. A box side-length of about 20 Å is a compromise between these two opposite requirements (for box size effects, see also discussion in section IIIC, first paragraph).

In Figure 3, we show the PMF's for the TRP−HIS unbound complex in vacuo, CCl_4, MeOH, DMSO, and water. All the color figures are available in postscript format upon request to the corresponding author. The average error on the PMF is evaluated as prescribed in section IIC and is reported in Table

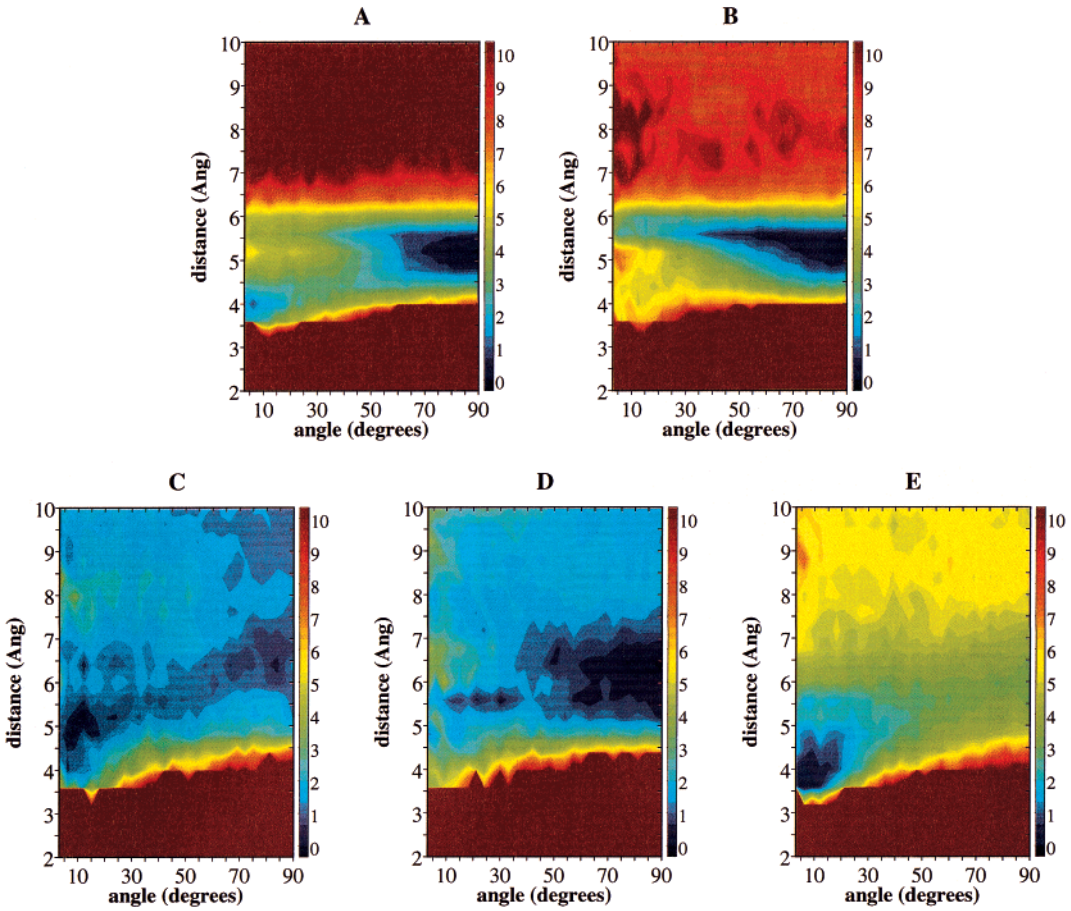

Figure 3. Potential of mean force for the TRP−HIS unbound complex in vacuo (A), CCl_4 (B), MeOH (C), DMSO (D), and water (E) as a function of the ring centroid distance (*Y* axis) and of the angle between the ring planes of TRP and HIS (*X* axis). On the right side of the pictures, the chromatic energy scale is shown in units of kJ mol^{-1}. The brown regions correspond to energies greater than 10 kJ mol^{-1}.

TABLE 3: σ_N Values (N is the number of the chunks) for the Different Runs (see text for details)[a]

C_a-C_b	3.8	5.0	6.5	no bond
vacuum	0.44, 1.27	0.59, 1.06	0.54, 1.28	0.39, 0.90
CCl_4	0.38, 0.93	0.39, 1.14	0.67, 1.49	1.07, 1.57
MeOH	0.71, 1.99	0.36, 1.14	0.51, 1.36	0.59, 2.03
DMSO	0.48, 1.18	0.42, 1.05	0.41, 1.08	0.80, 1.64
water	0.58, 0.91	0.46, 0.88	0.38, 1.23	0.93, 1.46

[a] The first number in each entry is σ_2 ($N = 2$), the second number is σ_5 ($N = 5$). C_a-C_b (in Å) is the constrained distance (see section III) of the TRP−HIS bound complexes. "No bond" label refers to the runs for the TRP−HIS unbound complexes. All values are given in kJ mol^{-1}.

3 for both the bound and unbound complexes. It should be noted that, due to the extended configurational space, the PMF's for the unbound pair are in general affected by a larger error with respect to the bound complexes that will be discussed later on. The PMF for the in vacuo run has a deep minimum at $R \approx 5.3$ Å and $\theta \approx \pi/2$, corresponding to T-shaped structures, and a secondary minimum at $R \approx 4$ Å and $\theta \approx 0$, corresponding to stacked structures. The T-shaped minimum is dominated by structures characterized by strong H-bond between the H_5 of TRP and N_1 of HIS (see Figure 1a). When the complex is immersed in a non polar solvent such as CCl_4, we observe two main effects: (i) the stacked minimum disappears, and (ii) the complex appears to be somewhat destabilized. The competing solute−solvent interactions affects mainly the minimum stabilized by dispersion interactions, i.e., the stacked minimum, while having a very little impact on the T-shaped minimum determined by the strong electrostatic interactions of the N_1(HIS)−H_5(TRP) H-bond. Indeed, electronic effects (charge transfer, cloud polarization or non conventional H-bonding[2]), while being certainly important in many instances, do not appear to be a decisive factor for stabilizing T-shaped arrangements for the TRP−HIS complex.

To the opposite end of the polarity scale, i.e., TRP and HIS in water (Figure 3E), the minimum relative to the T-shaped complex is completely wiped out, and only the stacked minimum survives. The competition between the solute−solvent and solute−solute electrostatic interactions inhibits the formation of T-shaped complexes. Further, the destabilization of the complex is much larger in water than in CCl_4 because the most stable minimum, the T-shaped complex, has been suppressed from the PMF. We remark that our results are in agreement with the observed trends for aromatic−aromatic interactions in proteins, where stacked structures are found to be the preferential arrangement for residues exposed to the solvent (i.e., water)[1,5,8] while T-shaped arrangements are found in the protein hydrophobic core.[1]

The PMF's relative to MeOH and DMSO (Figure 3C,D) are practically structureless with barely detectable minima for stacked (MeOH) and T-shaped (DMSO) structures with well depths on the order of the statistical error (see the energy scale in Figure 3 and the entries in column 5 of Table 3). One must therefore conclude that the TRP−HIS complex is unstable in these solvents at 300 K, either in the stacked or T-shaped forms. If the dielectric constant were the driving factor for determining the shape of the PMF in solution, one would not expect such a

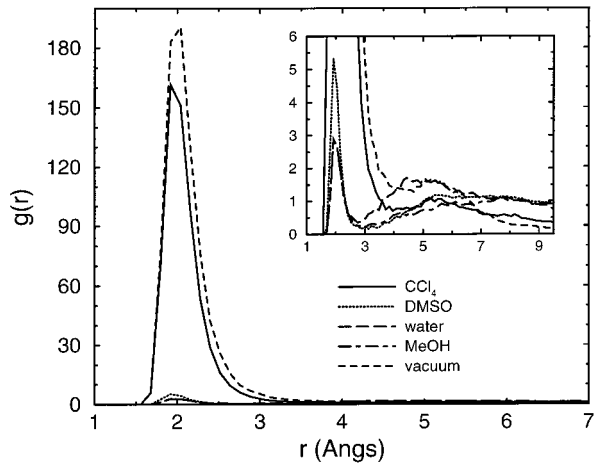

Figure 4. Radial distribution functions of the N_1(HIS)−H_5(TRP) pair of the TRP−HIS unbound complex in vacuo, CCl_4, MeOH, DMSO, and water. In the inset, the region $0 < g(r) < 6$ is shown.

destabilization of the complex but, rather, a continuous destabilization of the T-shaped form in favor of the stacked one, with increasing dielectric constant, that is in going from CCl_4 to MeOH, DMSO, and finally water. What we observe is stability in water (stacked form) and in CCl_4 (T-shaped form) and instability in MeOH and DMSO. It is clear that there must be some other factor besides the dielectric constant in determining this trend. The amphiphilic character of MeOH and DMSO could be a possible explanation for the observed results: the solute−solvent interactions due to the hydrophobic part of the solvent destabilize the stacked structures (as observed for CCl_4), while the hydrophilic moiety destabilizes the T-shaped minimum (as observed for water). The net effect of this concurrent destabilizations is the disappearance of stable complexes.

The importance of the solute−solute N_1(HIS)-H_5(TRP) H-bond in determining the pattern of the PMF can be inferred by inspection of Figure 4, where we show the radial distributions function for this specific pair in vacuo and in the different solvents. The intensity of the H-bond peak corresponding to the in vacuo sample is greater than that relative to the CCl_4 sample. This is consistent with the fact that the T-shaped minimum is slightly destabilized in CCl_4 because of the competition of solute−solute and solute−solvent interactions. The presence of a polar moiety in the solvent, as in MeOH, DMSO and water, induces an impressive lowering of the intensity of the H-bond peak (see inset of Figure 4). Note that H-bond donors/acceptors, like MeOH and water, induce a larger decrease of the intensity of the H-bond peak with respect to H-bond acceptors, like DMSO. In Figure 5a, we show the radial distribution functions between the polar hydrogen H_5 of methyl-indole (see Figure 1a) and the oxygen atom of DMSO, MeOH, and water. The larger intensity of the H-bond peak observed for DMSO and MeOH with respect to the water is consistent with the fact that, in these solvents, TRP and HIS tend to be dissociated, thereby favoring solute−solvent interactions. In water, the intensity of the H-bond peak is smaller because the stacked complex, which is less accessible for H-bonding by the solvent molecules with respect to the dissociated pair, is much more stable, as confirmed by the PMF. A similar trend is observed in the pair distribution functions between the nitrogen N_1 of methyl-imidazole (see Figure 1a) and the polar hydrogens of MeOH and water, shown in Figure 5b.

Given the importance of microsolvation effects in the PMF of the TRP−HIS complex, as revealed by our simulations, we investigated whether ab initio calculations using continuum dielectric models could still reproduce the relative stability of the T-shaped and stacked forms in water. To this end, we have performed single-point IPCM[12] calculations using the standard implementation in the Gaussian98 package[39] on these two structures, named AS1 and ATH1 as in ref 15. The calculations were done at the MP2 level of theory with counter-poise corrections[15] and using a 6-31G(d) basis set.

Previous studies have shown that the 6-31G(d) basis set yields solvation energies of small polar or non polar organic molecules in water that differ at most by 4 kJ mol^{-1} from those obtained using a 6-311+G(3df,2p) basis set (see for example Figure 2 of ref 11). Moreover, as remarked in ref 40, to the second order in the MP expansion, small basis sets such as the 6-31G(d), due to cancellation errors, yield for aromatic−aromatic interactions (for both stacked and T-shaped forms) stabilization energies that are in fair agreement (within 6 kJ mol^{-1}) with the energies obtained using accurate coupled cluster calculations with large basis sets. According to in vacuo ab initio calculations at the MP2/6-31G(d) level of theory, the stabilization energies of the AS1 and ATH1 structures are approximately the same (see Table 2 of ref 15). On the contrary, at the same level of theory, the IPCM stabilization energy of the T-shaped complex in water is about 41.1 kJ mol^{-1} compared to the value of 16.0 kJ $mol^{-1}$of the stacked one. Accordingly, T-shaped complexes in water are predicted to be strongly stabilized with respect to stacked forms, which is hardly surprising given the large value of the dipole of the complex ATH1 in comparison to that of AS1 (see Table 4 of ref 15). This is in striking contrast with experimental indications and with the results of our molecular dynamics simulations.

B. Selection of the Constrained Distances. In the constrained systems (Figure 1b), TRP and HIS interact while being attached to a rigid structure through an aliphatic carbon. In proteins, the $C_\alpha-C_\alpha$ distance for two interacting aromatic residues varies from 3.8−3.9 Å (consecutive residues) up to about 10 Å for pair of residues linked to different secondary structure elements. We have hence selected three distances, approximately corresponding to the minima of the free energy as a function of the distance between the C_α (C_a, C_b) carbons of the unconstrained pair in dielectrics at the extrema of our polarity scale, namely, in water and in vacuo. In principle, this free energy could be determined with a standard molecular dynamics simulation by computing the radial distribution function for the C_a-C_b pair, selecting a box size such as to minimize the size effects while at the same time minimizing the sampling of the configurational space, as we did for the unbound complex. In practice, preliminary calculations in these conditions have convinced us that the extra flexibility introduced by adding the C_α carbon expands the conformational space of the unconstrained pair to a level where the convergence of that distribution function needs simulations of the order of tens of nanoseconds. We therefore use an umbrella sampling[41,42] technique relative to the "reaction" coordinate given by the distance x between the α-carbons (C_a-C_b in Figure 1b).

To this end, we introduce a soft harmonic bias potential of the kind $V_b = K_{bias}(x - x_n)^2$, where K_{bias} and x_n are the force constant and the equilibrium distance, respectively. The force constant, $K_{bias} = 1$ kcal mol^{-1} $Å^{-2}$, is chosen so as to yield amplitudes of the order of 2 Å at 300 K. To cover the entire range from 3 Å up to 10 Å, we have done a series of seven simulations where x_n is taken equal to $2 + n$ Å, with $n = 1, 2, ..., 7$. Therefore, the overlapping region for two adjacent runs is about 1 Å. The PMF $W_n(x)$ in a given distance window has been standardly calculated by reweighting for the corresponding

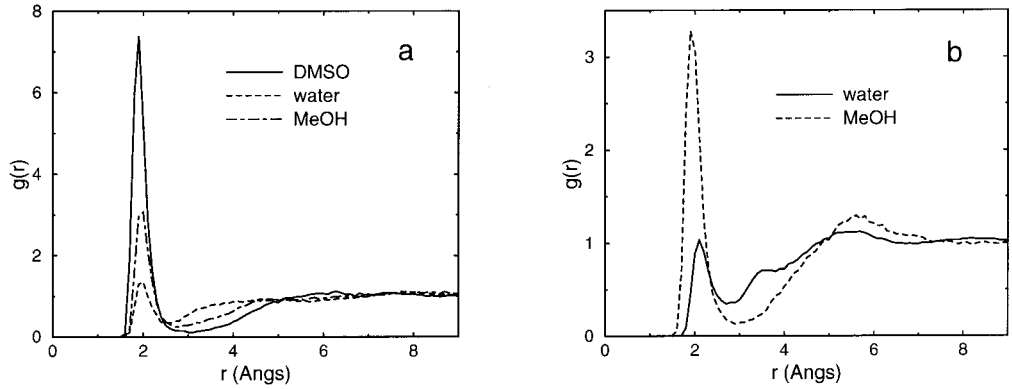

Figure 5. (a) Radial distribution functions between the polar hydrogen of TRP (H_5 in Figure 1a) for unbound complex solutions and the oxygen atom of MeOH (dot−dashed line), DMSO (solid line), and water (dashed line). (b) Radial distribution functions between the N_1 atom of HIS (see Figure 1a) and the hydrogen atoms of water (solid line) and MeOH (dashed line).

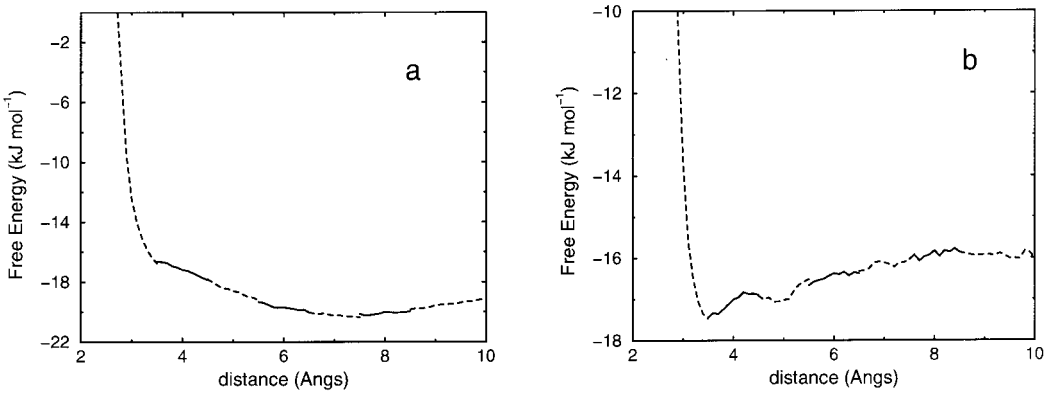

Figure 6. Potential of mean force (calculated by umbrella sampling method) in vacuo (picture a) and in water (picture b) as a function of the C_a-C_b distance. For each distance window, the range ($x_n - 0.5$ Å, $x_n + 0.5$ Å) is shown (see text for details). Free energies in adjacent windows are drawn as alternate solid and dashed lines.

bias potential the distribution function computed from molecular dynamics of the biased system. $W_n(x)$ is joined to that of the subsequent window $n + 1$ by minimizing the function $F = \int_n^{x_{n+1}}[W_n(x) - W_{n+1}(x)]^2\,dx$. In Figure 6a,b we show the PMF's for in vacuo and water, respectively. In the figures, the PMF's relative to adjacent windows are drawn with different line styles. In water, we detect two shallow minima at 3.5 Å and 4.9 Å. In vacuo, we find only one broad and shallow minimum in the range 6−8 Å. It is apparent that the preferential C_a-C_b distance (i.e., that occurring in the most stable complexes) in water is shorter than that in vacuo. In water, as discussed before, the stacked arrangement is favored, and stacked structures are compatible with relatively short C_a-C_b distances, whereas in vacuo or in solvents with low dielectric constant, the T-shaped structure is favored, and in this structure, the C_α carbons are distant. On the basis of the results obtained on the unbound complex in water with the two minima at 3.5 and 4.9 Å and in vacuo with the single broad minimum at ∼6−8 Å, we have therefore chosen the distances of 3.8, 5.0, and 6.5 Å for the runs on the constrained systems. These values covers the "contact range" between aromatic complexes. 3.8 Å is in fact approximately the minimum distance between the α carbons of two consecutive residues in proteins and is near to the primary minimum of water (see Figure 6b). The distance of 5.0 Å corresponds to the secondary minimum for the C_a-C_b distance in water. Finally, the distance of 6.5 Å, near the minimum for the in vacuo simulation (see Figure 6a), should be a value that favors structures typical of non polar environment.

C. Potential of Mean Force and Structural Properties of the Bound Complex. The distance constraint is implemented by adding the stretching potential $V_b = K_c(R - R_0)^2$, where R is the actual C_a-C_b distance and R_0 is the C_a-C_b constrained distance (3.8, 5.0, or 6.5 Å). The force constant K_c is chosen to be 100 kcal mol^{-1} Å^{-2}. This yields fluctuations of the distance R of about 0.3 Å, a value of the order of the Debye−Waller factor for the backbone atoms in proteins. In all cases, the simulation box is around 20 Å (see section II). The C_a-C_b distance is therefore in all circumstances well below $L/2$, and we may hence assume that the finite size effects on the PMF for the bound complexes should be small. To verify this assumption, we have done a simulation of CCl_4 in the least favorable case, namely, with R_0 set to 6.5 Å, but in a cubic box with an average side-length of 30.05 Å containing 163 solvent molecules. The thermodynamic conditions and the length of the run where identical to those of the smaller sample. The general pattern of the PMF is unchanged in going to the larger sample. In fact, the average difference of the PMF computed with the large and small samples was found to be 1.19 kJ mol^{-1}, i.e., on the order of the statistical error (see Table 3).

In Figure 7, we show the PMF computed in vacuo and in the four solvents for the bound complex with $R_0 = 3.8$, 5.0, and 6.5 Å. We recall that in vacuo, the most stable complex structure for the unbound TRP−HIS pair (see Figure 3A) was the T-shaped arrangement. For the bound complex with $R_0 = 6.5$ Å (Figure 7A), the situation is reversed, and the T-shaped structure occurs as a secondary minimum with a corresponding strong stabilization of the stacked structure. The stacked bound complex increases steadily its stability as R_0 is decreased. At $R_0 = 5.0$ Å, the T-shaped minimum is reduced to a shallow and high-energy region, and at 3.8 Å, there is no sign of a stable

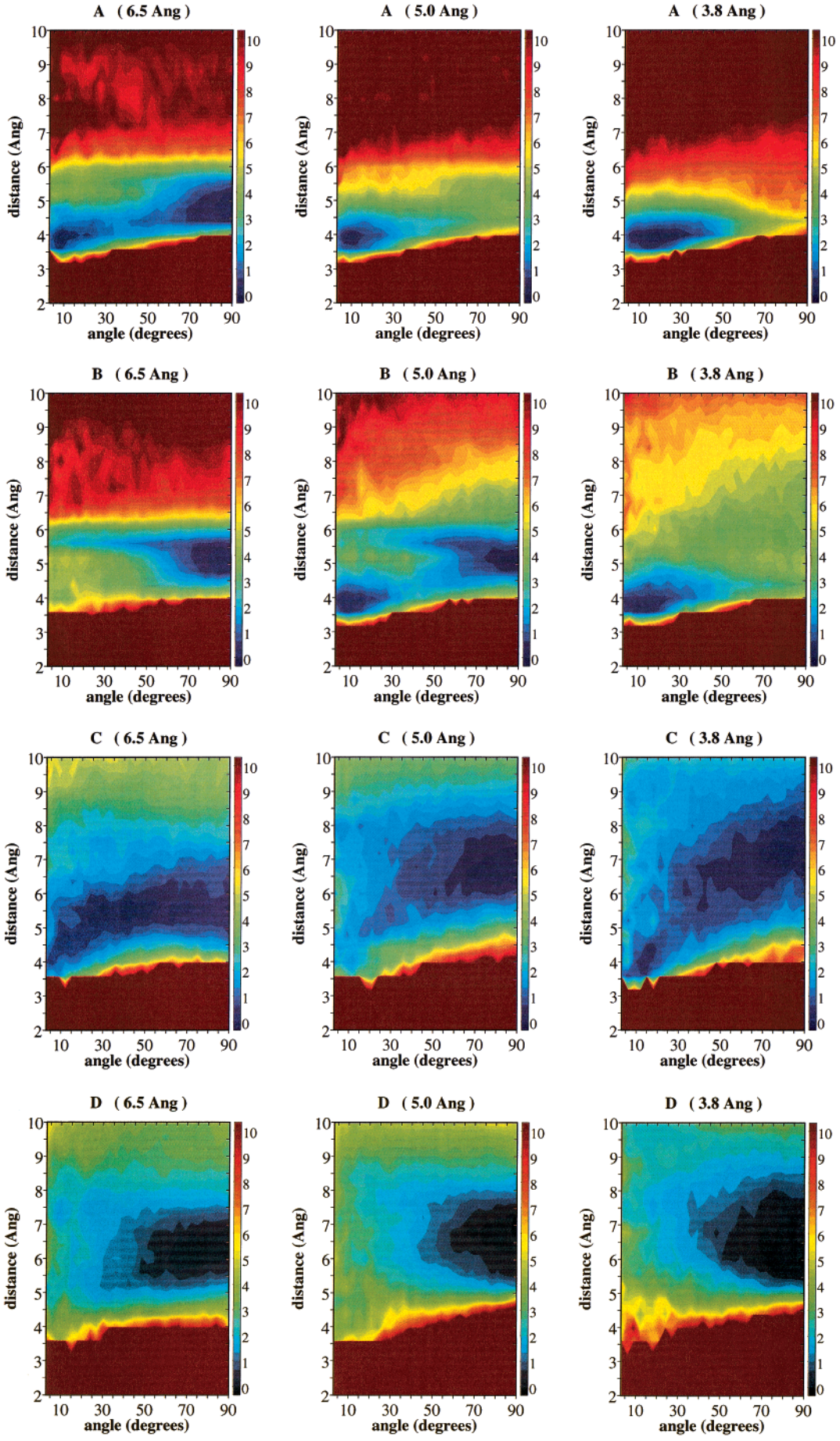
A (6.5 Ang)
A (5.0 Ang)
A (3.8 Ang)
B (6.5 Ang)
B (5.0 Ang)
B (3.8 Ang)
C (6.5 Ang)
C (5.0 Ang)
C (3.8 Ang)
D (6.5 Ang)
D (5.0 Ang)
D (3.8 Ang)
distance (Ang)
angle (degrees)

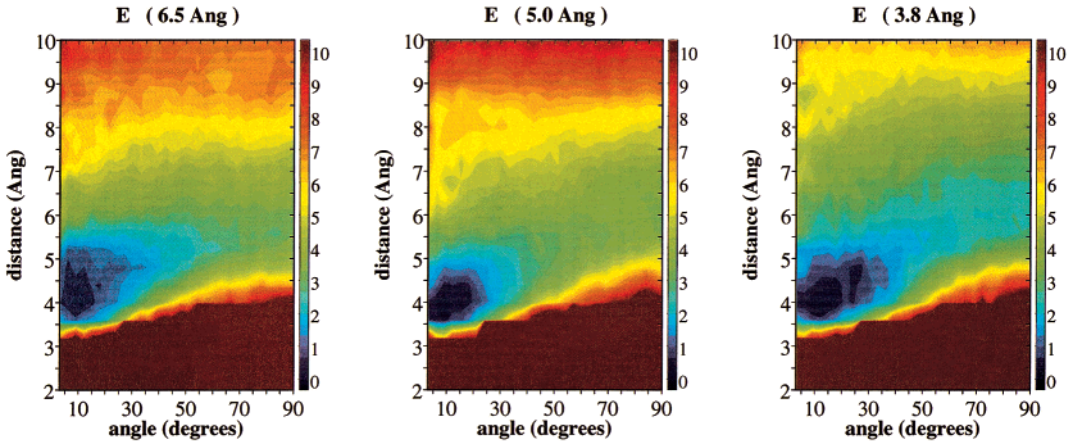

Figure 7. Potential of mean force for the TRP−HIS bound complex in vacuo (A), CCl_4 (B), MeOH (C), DMSO (D), and water (E) as a function of the ring centroid distance (*Y* axis) and of the angle between the ring planes of TRP and HIS (*X* axis). On the right side of the pictures, the chromatic energy scale is shown in units of kJ mol^{-1}. The brown regions correspond to energies greater than 10 kJ mol^{-1}. The different C_a-C_b constrained distances are reported on the top of the pictures.

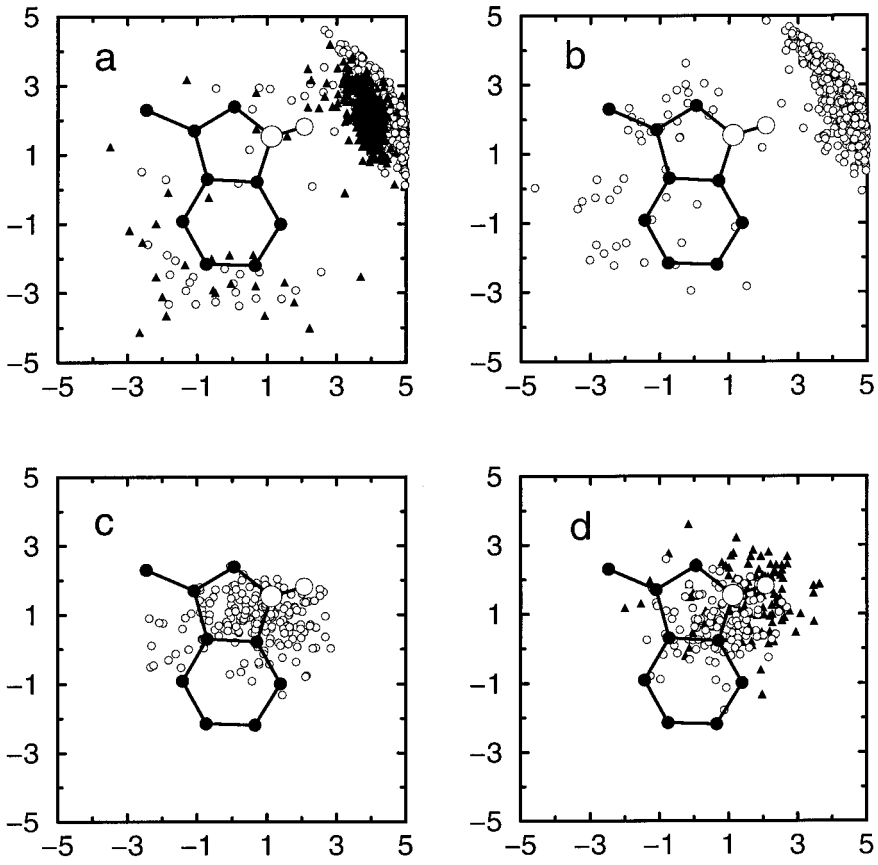

Figure 8. Distribution of the HIS ring centroid (open circles) on the TRP ring plane (shown in the pictures) for the unbound complex (picture a) and for the bound complex at the constrained C_a-C_b distances of 6.5 (picture b), 5.0 (picture c), and 3.8 Å (picture d) in CCl_4. "a" and "b" refer to T-shaped structures, while "c" and "d" to stacked ones. In the "a" and "d" pictures, the distribution of the N_1 HIS atom is also reported (triangles). The big open circles correspond to the polar hydrogen and to the nitrogen of TRP. The distances (*X* and *Y* axes) are in Å.

T-shaped arrangement, while only the stacked structure survives. In CCl_4 (Figure 7B), the solvent effect, i.e., the solubilization of the stacked complex, competes with the effect of the constraint which, on the contrary, tends to stabilize the stacked structures. At $R_0 = 6.5$ Å the T-shaped form is by far the most stable structure and is still present at $R_0 = 5.0$ Å, where the energy difference with respect to the more stable stacked form is less than 2 kJ mol^{-1}. At $R_0 = 3.8$ Å, the effect of the bond constraint prevails, and the stacked form is the only observed. In Figure 8, we show the distribution of the centroids of the HIS ring (open circles) projected on the TRP ring plane for configurations occurring in correspondence of the minimum structures in CCl_4. The reported configurations are selected using a window of $\Delta R \approx 1$ Å and $\Delta\theta \approx 20°$ around the minimum. In Figure 8a, the triangles represent the projection on the TRP ring plane of the coordinates of the nitrogen N_1 of HIS (see Figure 1b), which is involved in the solute−solute H-bond in T-shaped structures. As expected, for the unbound complex (Figure 8a) and for the largest distance in the bound system (Figure 8b), where the T-shaped form is dominant (see Figures 3B and 7B),

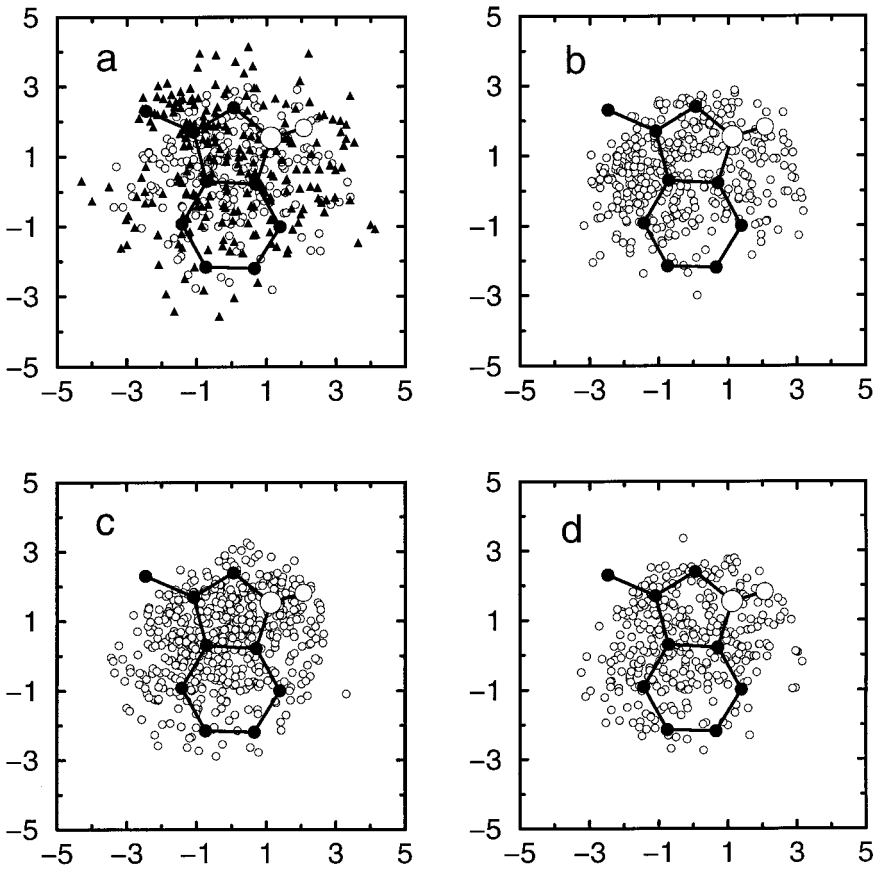

Figure 9. Distribution of the HIS ring centroid (open circles) on the TRP ring plane (shown in the pictures) for the stacked unbound complex (picture a) and for the stacked bound complex at the constrained C_a-C_b distance of 6.5 (picture b), 5.0 (picture c), and 3.8 Å (picture d) in water. In the "a" picture, the distribution of the N_1 HIS atom is also reported (triangles). The big open circles correspond to the polar hydrogen and to the nitrogen of TRP. The distances (*X* and *Y* axes) are in Å.

the centroid of the HIS lies preferentially on the side of the polar hydrogen of TRP, and its distribution almost overlaps to that of N_1. The distributions at $R_0 = 3.8$ and 5.0 Å (Figure 8c,d) refer to the stacked structures. It can be seen that the centroid of the HIS is mostly on the five-membered ring of TRP and is slightly shifted toward the polar hydrogen. The reason for this can be understood by inspection of Figure 8d, where, for $R_0 =$ 3.8 Å, the distribution of the HIS centroid is shown along with that of the N_1atom. Again N_1 lies preferentially above the polar hydrogen of TRP yielding a semieclipsed stacked structure, stabilized by the electrostatic interaction between the atoms N_1 of HIS and H_5 of TRP.

Going back to the PMF's of Figure 7, we remark that, for short constraint distances, intermolecular complexes are less stable. A dissociated or weakly interacting state for TRP and HIS is more probable when the C_a-C_b distance is small, while this dissociated state is less likely to occur when the C_α carbons are far apart. This behavior is quite general for solvents with low dielectric constant. It is in fact observed for CCl_4, MeOH, and even DMSO (Figure 7B−D). This apparently not obvious result can be explained on the basis of the behavior of the free energy as a function of the C_a-C_b distance for the unconstrained pair in vacuo reported in Figure 6a: large distances in generally favors the stable T-shaped complex thereby inhibiting dissociation.

In water, as already observed for the TRP−HIS unbound complex, the stacked structure is the only stable arrangement surviving the solubilization process. Here, large C_a-C_b distances, which tend to stabilize the T-shaped complexes in vacuo and in CCl_4, are unable to reverse the equilibrium stacked form ⇌ T-shaped form toward the latter. In water, at $R_0 = 6.5$ Å, the free energy landscape is quite similar to that registered at 5.0 and 3.8 Å or for the unbound complex (see Figures 7E and 3E). We also observe that dissociation is less likely at the intermediate distance 5.0 Å, corresponding to the secondary minimum of the free energy for the unbound complex reported in Figure 6b. This behavior is different from that of CCl_4, where the largest constraint distance (6.5 Å) favors the stabilization of the complex. Another remarkable difference between bound complex structures in water and in CCl_4 (or in vacuo) concerns the nature of the stacked arrangements. In CCl_4 and in vacuo, the HIS ring plane is superimposed to the TRP ring so as to minimize the N_1(HIS)−H_5(TRP) distance. In Figure 9, we report the distribution of the HIS centroid on the TRP ring for structures corresponding to the stacked minimum in water. This distribution is rather insensitive to the constraint distance R_0. Here N_1 and H_5 are less likely to be in contact as they are solvated by the water molecules. Consequently, the distribution is less localized and slightly shifted toward the β carbon C_1 of TRP, i.e., on the opposite side of that observed for the stacked form in CCl_4.

The distance constraint slightly stabilizes the complexes in DMSO and MeOH (Figure 7C,D). In MeOH, the complex is about 6 kJ mol^{-1} and 4 kJ mol^{-1} below the dissociated state at $R_0 = 6.5$ and 5.0 Å, respectively. In the former case, there is no clear preferential angle θ, whereas in the latter, a T-shaped structure is dominant. At $R_0 = 3.8$ Å, the TRP and HIS pair is preferentially dissociated, and complexation occurs mostly in the stacked form.

In DMSO, we remark a constant preference toward T-shaped structures with stabilization increasing with decreasing R_0 distance. At $R_0 = 3.8$ Å, however, the free energy of the T-shaped complex is only about 4 kJ mol^{-1} below the dissociated state. The weak but consistent preference for the T-shaped arrangements exhibited by DMSO with respect to MeOH in both bound and unbound complexes could be rationalized as follows: the OH group of the MeOH can bind both the H-bond acceptor and donor ends of the solute, while the SO group of the DMSO can bind only the H-bond donor end. Because of the dual character (versus *H*-bond) of its polar end, MeOH solvates the T-shaped complexes more efficiently than DMSO does. This is reflected, for example, in the behavior of the H-bond peak in the solute−solute N_1(HIS)−H_5(TRP) $g(r)$'s of the unbound complexes, as previously discussed (see Figure 4 and discussion in section IIIA).

IV. Conclusive Remarks

In this paper, we have calculated the structural properties in solution of the TRP−HIS interacting pair. In particular, we have calculated the potential of mean force as a function of the centroid−centroid distance and of the angle between the normal to the two aromatic rings for the TRP−HIS pair in vacuo and in various solvents. Results have shown that T-shaped structures are favored in non polar solvents, while they are destabilized in solvents that can form strong H-bonds. These results appear to be in agreement with experimental observations in proteins. In our calculation, we observe a strong stabilization of the T-shaped structure for residues anchored to distant α-carbons. This feature appears to be consistent with the experimental observation that aromatic−aromatic T-shaped contacts link distinct secondary structural elements,[1] and hence, their α-carbons are very likely quite far. In water, we observe a complete reverse of the equilibrium T-shaped form ⇌ stacked form in favor of the latter.

In water, only stacked structures are stable irrespective of the distance between the two α-carbons. This result is consistent with experimental observations[4] relative to a quite large incidence of this kind of packing for amino−aromatic interactions of residues generally exposed to the solvent. The stabilization of the stacked form in the presence of water molecules has been recently observed in a theoretical study on the adenine−thymine pair.[43]

As a general consideration regarding solvation effects for the TRP−HIS pair, we can state that the stacked structures are strongly stabilized in solvents that do not have hydrophobic moiety and that can form strong H-bond such as water. Amphiphilic solvents, such as DMSO and MeOH, which have a polar and nonpolar part, destabilize both the stacked and the T-shaped structures. The obtained results show the importance of the atomic details of the solvent in determining the free energy for the solute−solute interactions. The general behavior for the solvation phenomena observed in our molecular dynamics simulations cannot be rationalized in terms of a single parameter, such as the dielectric constant. We actually found that accurate IPCM calculations are unable to predict the inversion of the T-shape⇄stacked equilibrium in water and they even predict a large stabilization of the T-shaped complex, which, in the light of experimental indications, seems to be unlikely.

Acknowledgment. This work was supported by the Italian Ministero dell'Università e della Ricerca Scientifica e Tecnologica (MURST), the Consiglio Nazionale delle Ricerche (CNR), and the European Union (Contract No. ERBFMGECT950017). We are grateful to Alessandro Giolitti of the Menarini *S.p.A.* and Antonio Guarna for their useful suggestions.

References and Notes

(1) Burley, S. K.; Petsko, G. A. *Science* **1985**, *229*, 23−28.
(2) Levitt, M.; Perutz, M. F. *J. Mol. Biol.* **1988**, *201*, 751−754.
(3) Perutz, M. F. In *Pioneering Ideas for the Physical and Chemical Sciences*; Proceedings of the Josef Loschmidt Symposium; Fleischhacker, W., Schönfeld, T.; Eds.; Vienna, Austria, 1995; Plenum Press: New York; pp 1−14.
(4) Mitchell, J. B. O.; Nandi, C. L.; McDonald, I. K.; Thornton, J. M.; Price, S. L. *J. Mol. Biol.* **1994**, *239*, 315−331.
(5) Brocchieri, L.; Karlin, S. *Proc. Natl. Acad. Sci.* **1994**, *91*, 9297−9301.
(6) Sponer, J.; Leszczynski, J.; Hobza, P. *J. Biomol. Struct. Dyn.* **1996**, *14*, 117−135.
(7) Sponer, J.; Leszczynski, J.; Hobza, P. *J. Phys. Chem.* **1996**, *100*, 5590−5596.
(8) Kratochvil, M.; Engkvist, O.; Sponer, J.; Jungwirth, P.; Hobza, P. *J. Phys. Chem. A* **1998**, *102*, 6921−6926.
(9) Møller, C.; Plesset, M. *Phys. Rev.* **1934**, *46*, 618−622.
(10) Miertus, S.; Tomasi, J. *Chem. Phys.* **1982**, *65*, 239−245.
(11) Cossi, M.; Barone, V.; Cammi, R.; Tomasi, J. *Chem. Phys. Lett.* **1996**, *255*, 327−335.
(12) Foresman, J. B.; Keith, T. A.; Wiberg, K. B.; Snoonian, J.; Frisch, M. J. *J. Phys. Chem.* **1996**, *100*, 16098−16104.
(13) Jorgensen, W. L.; Severance, D. L. *J. Am. Chem. Soc.* **1990**, *112*, 4768−4777.
(14) Cornell, W. D.; Cieplak, P.; Bayly, C. I.; Gould, I. R.; Kenneth, M.; Merz, J.; Ferguson, D. M.; Spellmeyer, D. C.; Fox, T.; Caldwell, J. W.; Kollman, P. A. *J. Am. Chem. Soc.* **1995**, *117*, 5179−5197.
(15) Gervasio, F. L.; Procacci, P.; Cardini, G.; Guarna, A.; Giolitti, A.; Schettino, V. *J. Phys. Chem. B* **2000**, *104*, 1108−1114.
(16) Rick, S. W.; Berne, B. J. *J. Am. Chem. Soc.* **1996**, *118*, 672−679.
(17) Rappé, A. K.; Goddard, W. A., III *J. Phys. Chem.* **1991**, *95*, 3358−3363.
(18) Rick, S. W.; Stuart, S. J.; Berne, B. J. *J. Phys. Chem.* **1994**, *101*, 6141−6156.
(19) Chelli, R.; Ciabatti, S.; Cardini, G.; Righini, R.; Procacci, P. *J. Chem. Phys.* **1999**, *111*, 4218−4228.
(20) Bayly, C. I.; Cieplak, P.; Cornell, W. D.; Kollman, P. A. *J. Phys. Chem.* **1993**, *97*, 10269−10280.
(21) Fox, T.; Kollman, P. A. *J. Phys. Chem. B* **1998**, *102*, 8070−8079.
(22) Lide, D. R. *Handbook of Chemistry and Physics*; CRC Press: Boca Raton, FL, 1998.
(23) Casteel, J. F.; Sears, P. G. *J. Chem. Eng. Data* **1974**, *19*, 196−200.
(24) Berendsen, H. J. C.; Postma, J. P. M.; von Gunsteren, W. F.; Hermans, J. In *Intermolecular Forces*; Pullman, B., Ed.; Reidel: Dordrecht, The Netherlands, 1981; p 331.
(25) Buckingham, A. D. *Proc. R. Soc. London, Ser. A* **1956**, *238*, 235.
(26) Parrinello, M.; Rahman, A. *Phys. Rev. Lett.* **1980**, *45*, 1196−1199.
(27) Marchi, M.; Procacci, P. *J. Chem. Phys.* **1998**, *109*, 5194−5202.
(28) Nose, S. *J. Chem. Phys.* **1984**, *81*, 511−519.
(29) Essmann, U.; Perera, L.; Berkowitz, M. L.; Darden, T.; Lee, H.; Pedersen, L. G. *J. Chem. Phys.* **1995**, *101*, 8577−8593.
(30) Tuckerman, M. E.; Berne, B.; Martyna, G. *J. Chem. Phys.* **1992**, *97*, 1990−2001.
(31) Procacci, P.; Berne, B. J. *J. Chem. Phys.* **1994**, *101*, 2421−2431.
(32) Procacci, P.; Darden, T.; Paci, E.; Marchi, M. *J. Comput. Chemistry* **1997**, *18*, 1848−1862.
(33) Huenenberger, P. H.; McCammon, J. A. *J. Chem. Phys.* **1999**, *110*, 1856−1872.
(34) Hummer, G.; Pratt, L. R.; Garcia, A. E. *J. Phys. Chem.* **1996**, *100*, 1206−1215.
(35) Hummer, G.; Pratt, L. R.; Garcia, A. E. *J. Chem. Phys.* **1997**, *107*, 9275−9277.
(36) Hummer, G.; Pratt, L. R.; Garcia, A. E. *J. Phys. Chem. A* **1998**, *102*, 7885−7895.
(37) Hummer, G.; Pratt, L. R.; Garcia, A. E.; Berne, B. J.; Rick, S. W. *J. Phys. Chem. B* **1997**, *101*, 3017−3020.
(38) Chandler, D. *Introduction to Modern Statistical Mechanics*; Oxford University Press: New York, 1987.
(39) Frisch, M. J.; Trucks, G. W.; Schlegel, H. B.; Scuseria, G. E.; Robb, M. A.; Cheeseman, J. R.; Zakrzewski, V. G.; Montgomery, J. A., Jr.; Stratmann, R. E.; Burant, J. C.; Dapprich, S.; Millam, J. M.; Daniels, A. D.; Kudin, K. N.; Strain, M. C.; Farkas, O.; Tomasi, J.; Barone, V.; Cossi, M.; Cammi, R.; Mennucci, B.; Pomelli, C.; Adamo, C.; Clifford, S.; Ochterski, J.; Petersson, G. A.; Ayala, P. Y.; Cui, Q.; Morokuma, K.; Malick,

D. K.; Rabuck, A. D.; Raghavachari, K.; Foresman, J. B.; Cioslowski, J.; Ortiz, J. V.; Stefanov, B. B.; Liu, G.; Liashenko, A.; Piskorz, P.; Komaromi, I.; Gomperts, R.; Martin, R. L.; Fox, D. J.; Keith, T.; Al-Laham, M. A.; Peng, C. Y.; Nanayakkara, A.; Gonzalez, C.; Challacombe, M.; Gill, P. M. W.; Johnson, B.; Chen, W.; Wong, M. W.; Andres, J. L.; Gonzalez, C.; Head-Gordon, M.; Replogle, E. S.; Pople, J. A. *Gaussian 98*, revision A.5; Gaussian Inc.: Pittsburgh, PA, 1998.

(40) Hobza, P.; Selzle, H. L.; Schlag, E. W. *J. Phys. Chem.* **1996**, *100*, 18790−18794.

(41) Torrie, G. M.; Valleau, J. P. *J. Comput. Phys.* **1977**, *23*, 187−199.

(42) Frenkel, D.; Smit, B. *Understanding Molecular Simulations*; Academic Press: San Diego, CA, 1996.

(43) Kabeláč, M.; Ryjáček, F.; Hobza, P. *Phys. Chem. Chem. Phys.* **2000**, *2*, 4906−4909.